Journal of Nuclear Materials 390–391 (2009) 216–219

Contents lists available at ScienceDirect

Journal of Nuclear Materials

journal homepage: www.elsevier.com/locate/jnucmat

Fast camera imaging of dust in the DIII-D tokamak

J.H. Yu [a,*], D.L. Rudakov [a], A.Yu. Pigarov [a], R.D. Smirnov [a], N.H. Brooks [b], S.H. Muller [a], W.P. West [b]

[a] University of California-San Diego, 9500 Gilman Drive, MC 0417, La Jolla, CA 92093, USA
[b] General Atomics, P.O. Box 85608, San Diego, CA 92186-5608, USA

ARTICLE INFO

PACS:
52.40.Hf
52.55.Fa
52.25.Vy
52.70.Kz

ABSTRACT

Naturally occurring and injected dust particles are observed in the DIII-D tokamak in the outer midplane scrape-off-layer (SOL) using a visible fast-framing camera, and the size of dust particles is estimated using the observed particle lifetime and theoretical ablation rate of a carbon sphere. Using this method, the lower limit of detected dust radius is ~3 μm and particles with inferred radius as large as ~1 mm are observed. Dust particle 2D velocities range from approximately 10 to 300 m/s with velocities inversely correlated with dust size. Pre-characterized 2–4 μm diameter diamond dust particles are introduced at the lower divertor in an ELMing H-mode discharge using the divertor materials evaluation system (DiMES), and these particles are found to be at the lower size limit of detection using the camera with resolution of ~0.2 cm^2 per pixel and exposure time of 330 μs.

Published by Elsevier B.V.

1. Introduction

Dust is an important issue for future tokamaks because of safety issues such as tritium retention and the possibility of explosion hazard when dust is accidentally exposed to air or water [1]. Core and scrape-off-layer (SOL) contamination of the plasma by dust may also be a concern because ablated dust is a source of impurities which affects plasma performance. Studies of dust in DIII-D include the use of scattering from Nd:YAG lasers [2] which detects dust particles ranging in size from 0.1 to 1.6 μm estimated using a model based on Mie scattering [3]. Cameras have been used elsewhere to study dust, including the use of multiple cameras to determine 3D dust trajectories [4]. Here we present data from a fast-framing visible camera which is capable of detecting larger particles than those detected using laser scattering. We introduce a method of estimating dust size based on the observed dust lifetime and theoretical ablation rate of a carbon sphere, and the lower size limit of dust detection is verified by injecting calibrated dust of known size.

2. Experimental setup

The plasmas used here have a lower single-null magnetic configuration with plasma current I_p = 1.0–1.6 MA and toroidal field B_T = 2 T at the magnetic axis, with major radius R = 1.8 m and mean minor radius $\langle a \rangle$ = 0.6 m. Injected neutral beam power is P_{NBI} = 5–9 MW. The camera views a volume of ~1 m^3 in the outer midplane region of the tokamak through a midplane window located at toroidal angle $\phi = 90^\circ$ (see Fig. 1). An objective lens focuses the light onto the front face of an 8 × 10 mm coherent fiber-optic bundle, and light coming out the back of the fiber bundle is focused onto a Phantom v7.1 CMOS camera detector with 12-bit pixel depth. The spatial resolution of the detector is typically 256 × 256 with 1 pixel imaging approximately 0.2 cm^2 in the plasma. The images presented here are obtained without an optical filter, although dust has been observed using D_α (656 nm), CII (514 nm), CIII (465 nm), and ArI (697 nm) filters. Without a filter the camera optical system detects wavelengths in the range of 450–950 nm, and the frame rates used here range from 10^3 to 3 × 10^4 frames/s.

3. Dust trajectories

The 2D trajectories of particles are found from the camera data, and here we highlight qualitative differences between dust tracks detected during discharges following an entry vent into the vessel and dust tracks observed immediately following a disruption with a vertical displacement event (VDE). During the first few plasma shots following an entry vent, the camera detects a few thousand dust events per shot, which is more than an order of magnitude greater than typical dust detection rates later in the experimental campaign. Fig. 2(a) shows dust tracks from t = 300 to 500 ms during the second plasma shot following an entry vent, and the dust tracks are overlaid onto a background image of the plasma for reference. The vertical field-of-view corresponds to a distance of approximately 90 cm at the wall, and tracks are shown for particles which are detected for a minimum duration of 4 ms. The particles mainly move from right to left in the frame as shown by the arrow,

* Corresponding author.
E-mail address: jyu@ferp.ucsd.edu (J.H. Yu).

0022-3115/$ - see front matter Published by Elsevier B.V.
doi:10.1016/j.jnucmat.2009.01.053

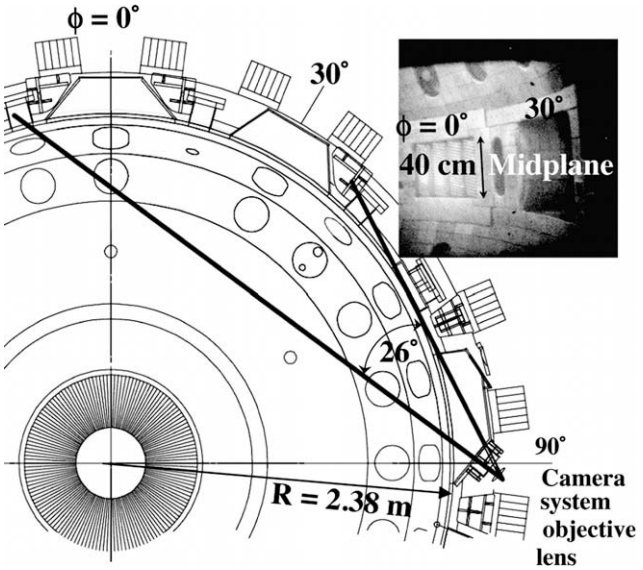

Fig. 1. Top view of the fast camera viewing region, shown bounded by the two solid lines; the inset shows a camera view inside DIII-D.

corresponding to the co-current direction. More particles are observed lower in the frame than higher, suggesting that most of the particles originate from the lower divertor region where unintentionally introduced dust settled following the entry vent.

During disruptions with VDEs, typically >10^3 dust particles are observed after the plasma moves upward and makes contact with the top of the vessel. Fig. 2(b) shows downward-directed trajectories of dust immediately following a disruption with a VDE. The median velocity of these particles is 100 m/s, and particles with velocity as high as 280 m/s are observed. Following disruptions with the plasma contacting the lower part of the center post, dust is seen moving in an upward direction pointed away from the plasma–surface contact region. This indicates that the downward-directed dust particles that follow disruptions with upward VDEs are not merely falling due to gravity, and possibly suggests that dust liberated from material surfaces may be initially accelerated due to micro-cracking from thermal stress [5] or due to particle interactions with rough surfaces [6].

4. Dust ablation

Dust particles are ablated due to heat and particle flux from the plasma, causing physical and chemical sputtering, as well as radiation-enhanced and thermal sublimation. The ablation rate shown in Fig. 3 includes these erosion processes and is used in the next section with the observed dust lifetime to estimate the size of camera-detected dust in DIII-D. In typical fusion plasmas, the dust temperature is sufficiently hot (>2500 K) such that the dominant dust erosion process is thermal sublimation, and material eroded from a carbon sphere is typically in the form of clusters [7]. The C_3 flux due to thermal sublimation from carbon dust at temperature T_d is given by

$$\Gamma_{C_3} = n_{C_3} v_T = \frac{P_{C_3} v_T}{T_d} = \frac{P_0 v_T}{T_d} \exp\left[\frac{\Delta H_{vap}}{R}\left(\frac{1}{T_0} - \frac{1}{T_d}\right)\right], \quad (1)$$

where the Clausius–Clayperon equation is used to relate the C_3 pressure P_{C_3} to the vapor pressure P_0 of carbon, $v_T = (T_d/M_{C_3})^{1/2}$ is the thermal velocity of the ejected C_3 clusters, ΔH_{vap} is the enthalpy of vaporization, T_0 = 3800 K is the carbon sublimation temperature, and R is the gas constant. The thermal sublimation rate is found from the effective flux [Eq. (1)] of all carbon atoms from a dust grain, which is based on the sum of fluxes due to C atoms and clusters up to C_5, with the sum weighted by the number of atoms in the ejected particle.

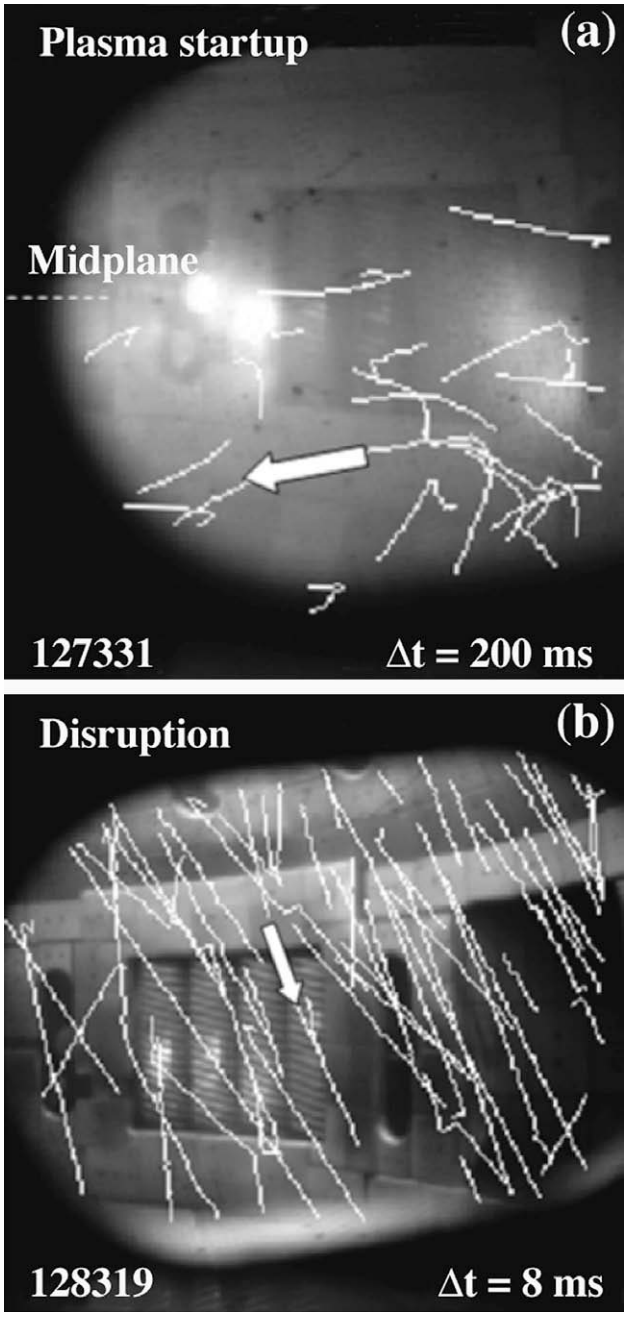

Fig. 2. Dust tracks (a) during the beginning of a plasma shot following an entry vent, and (b) after a disruption with an upward VDE.

5. Inferring dust size

The size of dust particles is estimated from the observed dust erosion time τ and the theoretical ablation rate $dR/dt(n_e, T_e)$ of a carbon sphere. A particle completely eroded in time τ with constant ablation rate has an initial size given by

$$R_d = -\eta\tau \frac{dR}{dt}(n_e, T_e), \quad (2)$$

where η is the vapor shielding factor [8] which we take as 0.7. Eq. (2) is used to estimate dust size. With a single camera the exact ra-

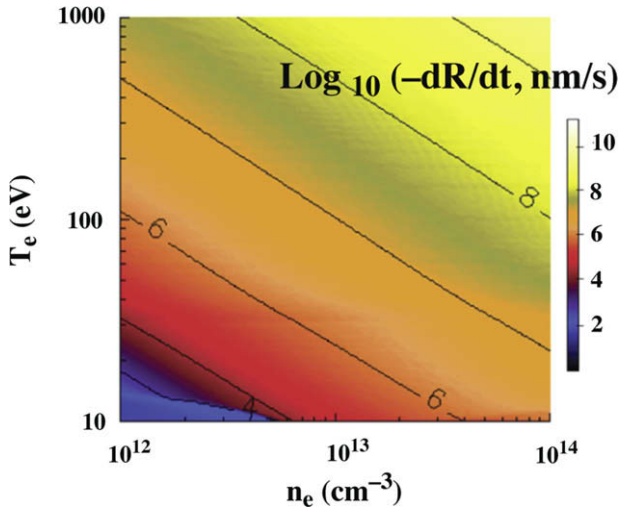

Fig. 3. Theoretical ablation rate for a carbon sphere, which is used with measurements of dust lifetime to estimate dust size.

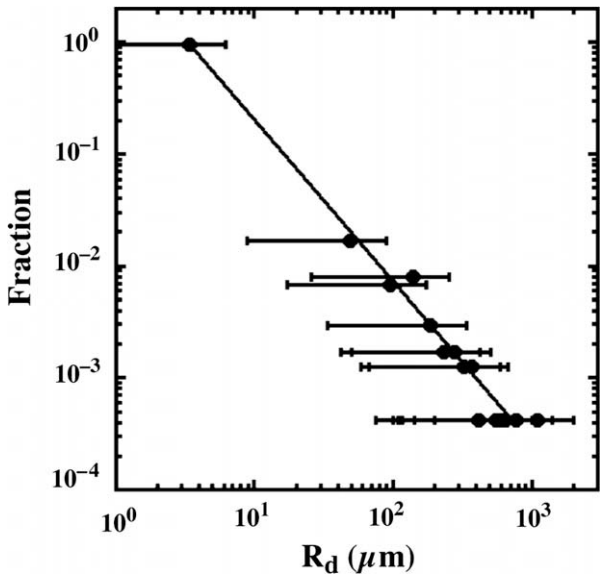

Fig. 4. Dust size probability distribution function for events detected by the fast camera. The solid line is a power law fit with $f \propto R_d^{-1.4}$.

dial location of the dust particle is unknown, and thus the plasma parameters (n_e, T_e) which determine dR/dt are unknown. Edge localized modes (ELMs), however, eject particles and heat into the SOL, and transport plasma with approximate pedestal parameters to the dust particle. Thus, we use the plasma pedestal values (typically $n_{e,ped} = 3 \times 10^{13}$ cm^{-3} and $T_{e,ped} = 400$ eV) to determine dR/dt. Here we neglect the ELM decay in the SOL, and thus the above values may be somewhat exaggerated. To determine τ, we use the interaction time of an ELM with the dust particle until the particle is completely destroyed. Most dust particles are destroyed within a single ELM, however, the largest observed particles with inferred radius ~1 mm survive up to 12 ELMs. For particles that interact with multiple ELMs, we assume that the ablation rate between ELMs is negligible and use the cumulative interaction time of the particle with ELMs to determine τ. Particles that survive multiple ELMs are fairly large with inferred radii $R_d \geqslant 80$ μm, and the ablation of these particles is dominated by ELMs. For example, a particle interacting with pedestal plasma transported by an ELM erodes $10^3\times$ faster than a particle in a $T_e = 10$ eV SOL plasma with no ELMs. However, the majority of observed dust particles have a short lifetime compared to the time between ELMs, and are destroyed even in the absence of ELMs presumably because they are sufficiently small to be ablated by the SOL plasma, or possibly because the particle moves toward the separatrix. These particles are assumed to be small, and when constructing the size distribution function they are included in the radius bin corresponding to the smallest inferred size from ELM–dust interactions.

Fig. 4 shows the count-based distribution of inferred dust size based on 2330 particles detected by the fast camera during H-mode operation in 12 plasma discharges. The smallest particles the camera detects are ~3 μm, and particles up to ~1 mm are also seen. The inferred size of these large particles may be overestimated, however, because estimates show that vapor shielding effects become significant for R_d larger than ~30–100 μm [9]. The horizontal error bars show variation in the inferred radius when n_e and T_e are varied by a factor of 2 from the pedestal values. The distribution roughly follows a power law scaling, suggesting universality in the mechanism of dust formation. The dust size distribution scales as $f(R_d) \propto R_d^{-1.4}$, and thus the putative dust mass distribution scales as $f(M_d) \propto M_d^{-0.5}$. Large particles ($R_d \geqslant 1$ mm) are rare and comprise $<10^{-3}$ of all detected dust events. However, despite their low detection rate, large particles contribute significantly to the total dust mass based on the probability distribution function scaling, because the total mass diverges as $R_d \to \infty$.

The lower limit of detectable particle size is tested by injecting calibrated diamond dust with diameter ranging between 2 and 4 μm from the divertor materials evaluation system (DiMES) [10]. The calibrated dust becomes mobile when the outer divertor strike point is swept over DIMES, causing the core carbon radiation to rise by a factor of 2. The camera images show that the injected dust is on the threshold of being detectable, as the dust is extremely difficult to see in the raw images. However, when the background image (the mean image obtained from surrounding frames) is subtracted the injected dust is observed with the dust luminosity marginally above the noise. Slightly larger sized graphite dust with median diameter of 6 μm has also been injected using DIMES in a separate experiment, and these particles could be detected by the fast camera without background subtraction. The calibrated dust injection experiment provides an independent check on the minimum inferred particle size obtained from the method based on dust lifetime and ablation rate.

Inferring dust sizes from the dust lifetime during ELM–dust interactions needs careful examination. ELMs have been shown to eject highly filamented plasma [11,12], and thus the actual interaction time between a hot filament and a dust particle is difficult to measure due to the complex spatial and temporal structure of ELM filaments. In addition, previous probe measurements have shown that during an ELM the plasma parameters decay with distance from the separatrix [13,14]. Assuming n_e and T_e decay by a factor of 2–3 in the SOL, the inferred dust radius decreases by a factor of approximately 10. Another concern is that the observed dust may not consist of pure carbon, while the theoretical ablation rate used to estimate dust size is calculated for carbon. A boron particle at 3000 K, for example, sublimates nearly 10× faster than a carbon particle at the same temperature [15]. The assumption of carbon composition for the dust modeling is reasonable, however, as the bulk of dust collected from the DIII-D vacuum vessel in previous studies is carbon [16]. Another possible issue is that blobs or ELM filaments colliding with a dust particle may change the dust velocity due to friction with flowing ions. If the dust particle rapidly moves out of the camera viewing volume within the time exposure for a single frame, a false measure of the particle lifetime would be obtained. However, estimates show that ELMs do not significantly move particles of the size that cameras are capable of detecting [17], and camera images show that ELMs do not appear

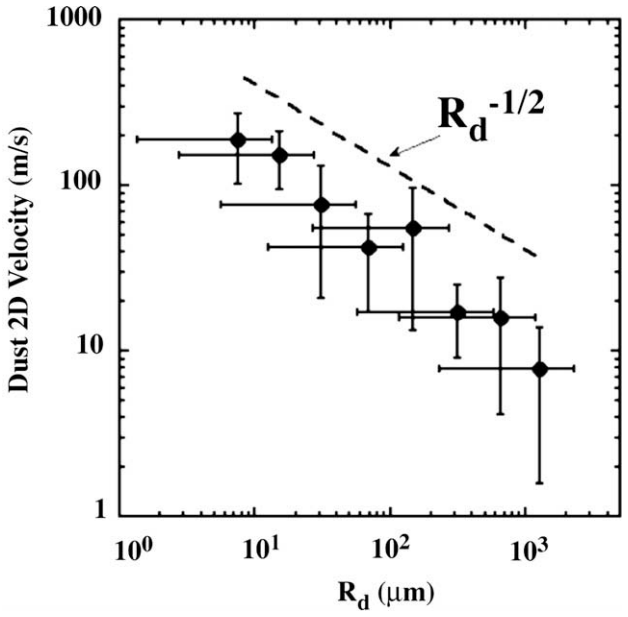

Fig. 5. Measured 2D dust velocity decreases with dust size, showing that particles with larger inertia experience less acceleration due to ion friction.

to significantly change dust velocities. Another assumption that may affect the accuracy of our estimates is that of the particles being spherical. The millimeter size particles are typically flakes with thickness much smaller than the length or width [16], so they may ablate quite differently from a sphere. Finally, the sublimation rate calculation is based on the assumption of thermal equilibrium of the dust particle. The time required to establish thermal equilibrium is estimated as $\tau_h = c_{pd} M_d \Delta T_d / (P_h - P_c)$, where P_h and P_c denotes heating and cooling power, respectively, and c_{pd} is the specific heat capacity of the dust. Estimates show that to raise the temperature of a particle of size $R_d > 100$ μm by $\Delta T_d = 500$ K, the heating time is comparable to the interaction time between an ELM and the particle. Thus, future work may include taking heat conduction of the dust particle into account and determining possible effects on ablation dynamics.

6. Dust velocity

The camera data is used to measure the dust velocity projected onto a plane perpendicular to the viewing direction, which is a lower limit on the actual 3D velocity magnitude. Fig. 5 shows that smaller particles move faster than larger particles, as expected, with the 2D-projected velocity ranging from <10 to ~300 m/s. The vertical bars represent the standard deviation of velocities for particles in each radius bin. In Fig. 5, only the initial particle velocity and radius are considered. For particles that survive multiple ELMs, a discrete velocity increase up to a factor of 3 is observed following the sudden ablation caused by an ELM. The 2D velocity data roughly agree with the $R_d^{-1/2}$ scaling predicted by a simple 1D analytic model of spherical dust particles accelerated due to ion drag in a uniform plasma, for a fixed distance between the dust origin and the measurement region [18]. DUSTT modeling shows that dust acceleration takes place mainly in the region near the divertor where parallel flow is largest, and that particles can reach ~1 km/s after rapid reduction in mass due to ablation [17]. Using existing cameras, particles with such high speeds may not be detectable because of their small size and due to lack of contrast.

7. Conclusions

Using a visible fast-framing camera, dust size in DIII-D is estimated based on the observed dust lifetime and theoretical ablation rate of a carbon sphere. Using this method, the count-based size distribution of dust roughly follows a power law scaling with the minimum inferred dust size detected by the fast camera of ~3 μm. Pre-characterized 2–4 μm diamond dust particles introduced at the lower divertor in an ELMing H-mode discharge using DiMES are at the lower size limit of detection, and provide an independent method of determining the minimum size of detected dust. Dust with inferred radius up to ~1 mm is observed. The detection rate of these large particles is low; however, these large particles can contribute significantly to the total dust mass inventory.

Acknowledgments

This work supported by the US Department of Energy under DE-FC02-04ER54698 and DE-FG02-07ER54917.

References

[1] G. Federici et al., Nucl. Fus. 41 (2001) 1967.
[2] W.P. West et al., Plasma Phys. Control. Fus. 48 (2006) 1661.
[3] R.D. Smirnov et al., Phys. Plasma 14 (2007) 112507.
[4] A.L. Roquemore et al., J. Nucl. Mater. 363–365 (2007) 222.
[5] S.I. Krasheninnikov, private communication.
[6] S.I. Krasheninnikov et al., Phys. Plasma 11 (2004) 3141.
[7] C.A. Klein et al., J. Appl. Phys. 65 (1989) 3425.
[8] P.B. Parks et al., Nucl. Fus. 34 (1994) 417.
[9] S.I. Krasheninnikov et al., Plasma Phys. Control. Fus. 50 (2008) 124054.
[10] D.L. Rudakov, J. Nucl. Mater. 363–365 (2007) 227.
[11] J.H. Yu et al., Phys. Plasma 15 (2008) 032504.
[12] A. Kirk et al., Phys. Rev. Lett. 96 (2006) 185001.
[13] J.A. Boedo et al., Phys. Plasma 12 (2005) 072516.
[14] D.L. Rudakov et al., Nucl. Fus. 45 (2005) 1589.
[15] Y. Tanaka et al., Phys. Plasma 14 (2007) 052504.
[16] W.J. Carmack et al., Fus. Eng. Des. 51&52 (2000) 477.
[17] A.Yu. Pigarov et al., Phys. Plasma 12 (2005) 122508.
[18] R.D. Smirnov et al., J. Nucl. Mater. 390–391 (2009) 84.